Empirical calibration of the λ4000 Å break[*]

J. Gorgas[1], N. Cardiel[1], S. Pedraz[1], and J. J. González[2]

[1] Departamento de Astrofísica, Facultad de Ciencias Físicas, Universidad Complutense de Madrid, 28040 Madrid, Spain
[2] Instituto de Astronomía, U.N.A.M., Apdo. Postal 70-264, 04510 Mexico D.F., Mexico

Abstract. Empirical fitting functions, describing the behaviour of the λ4000 Å break, D_{4000}, in terms of effective temperature, metallicity and surface gravity, are presented. For this purpose, the break has been measured in 392 stars from the Lick/IDS Library. We have followed a very detailed error treatment in the reduction and fitting procedures, allowing for a reliable estimation of the break uncertainties. This calibration can be easily incorporated into stellar population models to provide accurate predictions of the break amplitude for, relatively old, composite systems.

Key words: stars: fundamental parameters — galaxies: stellar content — techniques: spectroscopic — stars: atmospheres

1. Introduction

The spectroscopic study of the blue and near-UV region around λ4000 Å has proven to be a useful tool to investigate the stellar populations of composite stellar systems. Obviously, this spectral region is specially suited to detect the presence of young stars and therefore, to study star formation histories. Furthermore, in a pioneering work, Morgan (1959) already showed that the difference in intensity of the continuum level on the two sides of Hζ (λ3889 Å) in galactic globular clusters correlated well with metal abundance.

Although different absorption line-strength indices have been defined in this spectral range to understand the stellar composition of early-type objects (e.g., Faber 1973; Burstein et al. 1984; Rose 1984, 1994; Tripicco 1989; Worthey et al. 1994, hereafter W94; Jones &

Worthey 1995; Worthey & Ottaviani 1997; Vazdekis & Arimoto 1999), some of them are quite dependent on spectral resolution (and therefore velocity dispersion) and, in many cases, their use requires relatively high signal-to-noise ratios. In this sense, an interesting spectral index that avoids these problems is the λ4000 Å break. We have already demonstrated (Cardiel et al. 1998b) that this discontinuity can be measured with a relative error of ∼ 10% with a signal-to-noise ratio per Å ∼ 1. Thus, the break is well suited to be measured in faint objects or at low surface brightnesses. However, this advantage, due to the large wavelength interval employed in its definition, also translates into an important drawback: many absorption lines are included in the break bandpasses. Therefore, the behaviour of the break is expected to be complex.

In this work we are using the definition adopted by Bruzual (1983), who defined this spectral index as the ratio of the average flux density, F_ν (erg s^{-1} cm^{-2} Hz^{-1}), in two bands at the long– and short–wavelength side of the λ4000 Å discontinuity, in particular

$$D_{4000} = \frac{(\lambda_2^- - \lambda_1^-)}{(\lambda_2^+ - \lambda_1^+)} \frac{\displaystyle\int_{\lambda_1^+}^{\lambda_2^+} F_\nu \, \mathrm{d}\lambda}{\displaystyle\int_{\lambda_1^-}^{\lambda_2^-} F_\nu \, \mathrm{d}\lambda}, \qquad (1)$$

where $(\lambda_1^-, \lambda_2^-, \lambda_1^+, \lambda_2^+)$ = (3750, 3950, 4050, 4250) Å. Except for the combination of ν and λ, (due to the measurement method employed by Bruzual, in which the break was obtained from galaxy spectra plotted as F_ν versus λ), and for not being in logarithmic units, this definition resembles that of a color. Because of this, the D_{4000} can be considered as a pseudo-color. However, it must be pointed out that, compared to the classical color indices in this spectral range (like $U - B$), the 4000 Å break is much less sensitive to extinction by dust, and hence, it is more valuable to investigate the stellar content of galaxies. In particular, using the average interstellar extinction curve from Savage & Mathis (1979), the D_{4000} can be

corrected from internal reddening (and galactic extinction for objects at zero redshift) using the following expression

$$D_{4000}^{\text{corrected}} = D_{4000}^{\text{observed}} \, 10^{-0.0988 \, E(B-V)}. \qquad (2)$$

It is interesting to note that the break definition is still the same for redshifted objects, where the integral limits must be properly modified, and that absolute fluxes are not required. As a working expression, the 4000 Å break can be rewritten as

$$D_{4000} = \frac{\int_{4250\,(1+z)}^{4050\,(1+z)} \lambda^2 f_\lambda \, d\lambda}{\int_{3750\,(1+z)}^{3950\,(1+z)} \lambda^2 f_\lambda \, d\lambda}, \qquad (3)$$

where f_λ is the flux density per unit wavelength (in arbitrary units), and z is the redshift of the object being measured.

Up to date, many authors have employed the D_{4000} to study the stellar composition and star formation history of early-type galaxies (e.g. McClure & van den Bergh 1968; Spinrad 1980, 1986; Bruzual 1983; Laurikainen & Jaakkola 1985; Hamilton 1985; Dressler 1987; Dressler & Shectman 1987; Johnstone et al. 1987; Kimble et al. 1989; Dressler & Gunn 1990; Rakos et al. 1991; Charlot et al. 1993; Charlot & Silk 1994; Davidge & Clark 1994; Songaila et al. 1994; Belloni et al. 1995; Davidge & Grinder 1995; Cardiel et al. 1995, 1998; Abraham et al. 1996; Hammer et al. 1997; Barbaro & Poggianti 1997; Longhetti et al. 1998; Ponder et al. 1998). The reliable analysis of the break measurements rests on the comparison of the data with the predictions of stellar population models (e.g. Worthey 1994; Bruzual & Charlot 1996). So far, such predictions are computed by using either model atmospheres, or stellar libraries with a poor coverage of the atmospheric parameter space, especially in metallicity.

In this paper we present an empirical calibration of the λ4000 Å break as a function of the main atmospheric stellar parameters (namely effective temperature, surface gravity and metallicity) in an ample stellar library which covers an appropriate range of parameters to study relatively old stellar populations. One of the main advantages of using fitting functions to describe the behaviour of spectral indices is that they allow stellar population models to include the contribution of all the required stars, through a smooth interpolation in the space defined by the fitted stellar parameters. The usefulness of this approach has been demonstrated by the successful inclusion of similar fitting functions in recent evolutionary synthesis models (e.g. Worthey 1994; Vazdekis et al. 1996; Bressan et al. 1996; Bruzual & Charlot 1996).

It is important to keep in mind that the empirical calibration is only a mathematical representation of the break behaviour as a function of atmospheric stellar parameters, and that we do not attempt to obtain any physical justification of the derived coefficients.

We briefly review the previous works devoted to understand the D_{4000} in Sect. 2. The star sample is given
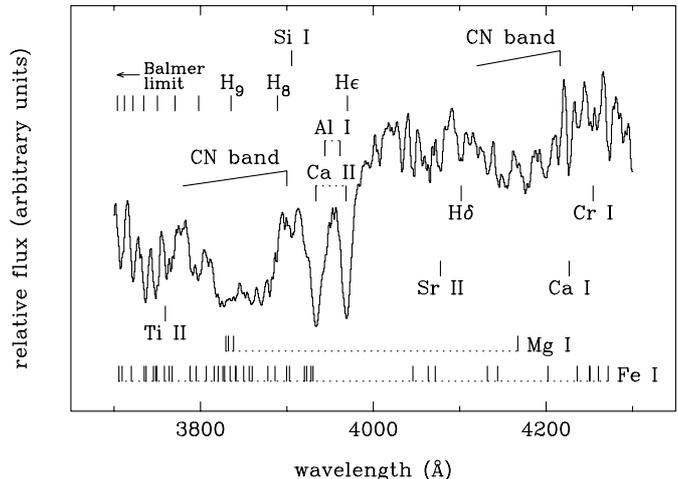
Fig. 1. Spectrum of the star HD 72324 (G9 III) in the region around the λ4000 Å break. As a reference, we have also plotted the most intense (EW > 200 mÅ) Fraunhofer lines from the sun (using the tabulated data from Lang 1974 —original source Moore et al. 1966—), together with the Balmer lines and two CN molecular bands (the central bandpass of the CN3883 index defined by Pickles 1985, and the absorption band of the S(4142) index employed by Smith et al. 1997) which can be found in this spectral range. The contribution of the atomic metallic lines, especially from Fe I and Mg I, becomes very important bluewards λ4000 Å

in Sect. 3. The observations and data reduction are described in Sect. 4, whereas Sect. 5 contains a description of the error analysis. In Sect. 6 we show the behaviour of the measured D_{4000} values as a function of the stellar atmospheric parameters. The fitting strategy and the resulting empirical function are presented in Sects. 7. Finally, in Sect. 8 we give a summary, providing a public FORTRAN subroutine written by the authors to facilitate the computation of the D_{4000} using the fitting function presented in this paper. Sections 4 and 5 are rather technical, due to the inclusion of a lengthy explanation of the data and error handling. We suggest the reader not interested in such details to scan Tables 1 and 2, and skip those sections.

2. Previous works: Understanding the D_{4000}

The λ4000 Å break is a sudden onset of absorption features bluewards 4000 Å which is clearly noticeable for stellar types cooler than G0 (see Fig. 3). In Fig. 1 we show a typical spectrum of a cool star in this spectral region, together with the identification of the most prominent spectral features. Considering the large wavelength range employed in the measurement of the D_{4000}, it is expected the strength of this discontinuity to be a function of the distribution of the continuum light in this region (governed by the effective temperature) modulated by the absorption line strengths (which must depend primarily on

both temperature and metallicity, and secondly on gravity). This behaviour converts the break in a potential tool to investigate composite stellar populations in early-type systems.

The relevance of the line-blanketing discontinuity near $\lambda 4000$ Å was the object of a systematic study by Wildey et al. (1962). These authors measured the *energy subtracted* in the spectra of some stars due to Fraunhofer lines, showing that the effect was important below $\lambda 4000$ Å. Van den Bergh (1963), and van den Bergh & Sackmann (1965) defined a break, Δ, as the ratio of the smoothed observed continuum at both sides of $\lambda 4000$ Å. These authors measured this break in a sample of 200 stars concluding that Δ depended both on stellar metallicity and $B - V$ color. Analogous discontinuity definitions, like $C(38 - 41)$ (McClure & van den Bergh 1968), and $\Gamma(38 - 41)$ (Carbon et al. 1982), have been also employed in the spectroscopic analysis of stars, star clusters and galaxies.

Using spectrophotometric stellar libraries, Bruzual (1983) and Hamilton (1985) studied the variation of the $\lambda 4000$ Å break with spectral types and luminosity classes (compare Fig. 3 in Bruzual with Fig. 6 in Hamilton). Both authors concluded that, as a function of temperature, the D_{4000} increases slowly for spectral types in the range from O5 to G0, and faster from G0 to M0, whereas the break decreases for the later types, M0 to M5. In addition, whilst for spectral types hotter than G0 the break does not depend on gravity, a clear dichotomy between main sequence stars on one hand, and giant and supergiant stars on the other, is apparent for lower temperatures. Given the scarcity of the employed stellar libraries, no dependence on metallicity could be obtained in these works.

From the analysis of moderate-resolution spectra of 950 galaxies in 12 rich clusters, Dressler & Shectman (1987) argued that, in composite stellar populations, the break is insensitive to changes in metal abundance, at least in the metallicity range spanned by their galaxy sample. This result was employed by Munn (1992) to conclude that the $CN - D_{4000}$ diagram is effective at separating metallicity and age effects on the integrated spectra of early-type galaxies. However, Kimble et al. (1989) obtained that the break correlated strongly with metallicity indicators, such as the Mgb index.

More recently, Poggianti & Barbaro (1997), working with Kurucz's models, have obtained a theoretical calibration of the break as a function of stellar parameters. They present (Fig. 1 in their paper) the behaviour of the D_{4000} in the ranges $5500 < T_{\mathrm{eff}} < 35000$ K, $0 < \log g < 5$, and $-2 < \log Z < 0$. This work clearly shows the strong dependence of the break on effective temperature, as previously reported from the studies based on stellar libraries, and quantifies, for a small sample of temperatures, the variation of the break as a function of metallicity and gravity. The D_{4000} is shown to be insensitive to metallicity for
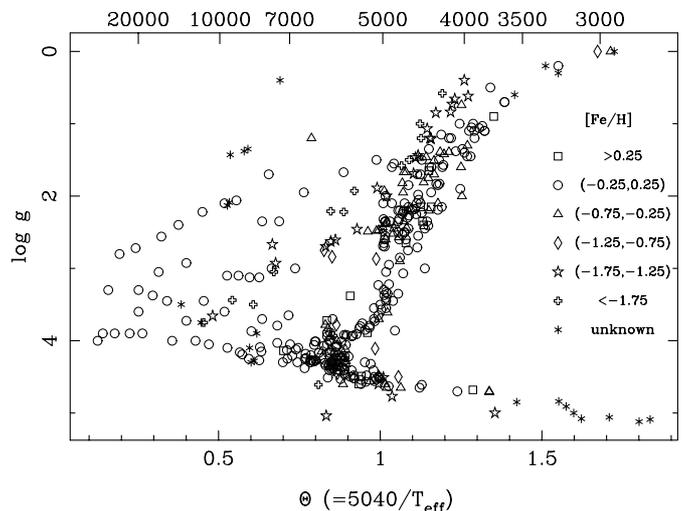
Fig. 2. Gravity–temperature diagram for the sample of stars used to derive the empirical fitting function. Different symbols are used to indicate stars of different metallicities, as shown in the key

hot stars ($T_{\mathrm{eff}} = 9000$ K), whereas the contrary is true for $T_{\mathrm{eff}} = 5500$ K. In addition, using the stellar spectra of Straizys & Sviderskiene (1972; note that these spectra are those also employed by Bruzual 1983), these authors obtain that, for stars with $3500 < T_{\mathrm{eff}} < 5500$ K, the D_{4000} always exhibits values above 2, with a maximum of 3 at $T_{\mathrm{eff}} = 4000$ K. Using this theoretical calibration, Barbaro & Poggianti (1997) have also elaborated an evolutionary synthesis model which predicts, in the integrated spectrum of a galaxy, the variation of the D_{4000} as a function of the star formation rate (SFR). More interestingly, they conclude that the break can be employed to yield the ratio of the SFR averaged over the last 5 billion years to the present SFR.

From all these previous works, it is quite clear that the D_{4000} is a suitable tool to face the study of stellar systems, in particular to reveal their stellar composition. However, a detailed empirical calibration, such as that presented in this paper, is needed to i) overcome the unavoidable uncertainties associated to the theoretical calibrations, ii) extend our understanding of the break behaviour for stars with $T_{\mathrm{eff}} < 5500$ K (note that these late-type stars constitute a fundamental ingredient in the modeling of old stellar populations), and iii) use in conjunction with other indices previously calibrated with the same stellar library.

3. Star sample

In order to derive a confident empirical calibration of the D_{4000}, we decided to measure this spectral feature in all the stars belonging to the Lick/IDS Library (Burstein et al. 1984; Faber et al. 1985; Burstein et al. 1986; Gorgas et al. 1993, hereafter G93; and Worthey et al. 1994).

The suitability of the Lick/IDS library to obtain empirical fitting functions has been widely demonstrated by the works of G83, W94, and Worthey & Ottaviani (1997), who, in overall, have derived analytical expressions for 25 spectral indices in the $4000 - 6000$ Å region. Trager et al. (1998), and references therein, have extensively shown the usefulness of the Lick/IDS absorption-line index system in the study of old stellar populations. In brief, the Lick/IDS library contains 460 stars of all spectral types and luminosity classes. Although a large fraction are field stars from the solar neighbourhood, members of open clusters (covering a wide range of ages) and galactic globular clusters (with different metallicities) are also included.

Table 1 lists the final data sample, which comprises 392 stars out of the original set of 424 objects with published atmospheric parameters in W94 (the remaining 32 stars presented high uncertainties in the derived measurements and were not included in order to guarantee the quality of the final dataset). The first two columns list the Henry Draper Catalog number, if any, and other common designation. The spectral type and luminosity class are given in the third column (see references at the end of the table). The following columns list the atmospheric parameters employed in this work. Most of them are those listed in the electronic table of W94. Since we wish to keep the consistency with the previous fitting functions for the Lick indices, we have been reluctant to change any atmospheric parameter. However, we have introduced new parameters for some of the stars which lack them in W94, and, in some cases, the original parameters have been improved using more recent or reliable data from the literature (see the description in the table notes). As a whole, effective temperature, gravity and metallicity data are finally available for 383, 382 and 354 stars, respectively.

To summarize, the Lick/IDS library spans the following ranges in atmospheric parameters: T_{eff} from 2747 to 21860 K, $\log g$ from 0 to 5.12, and [Fe/H] from -2.70 to 0.46. It is important to note that the star sample does not homogeneously cover the parameter space, being more densely populated in the metallicity interval -1.0 dex to $+0.5$ dex, whereas the gravity range is wider close to solar metallicity. A more important deficiency of the library is the paucity of hot stars. Since we are also interested in applying the derived fitting functions to the modeling of younger stellar populations, we have enlarged the sample with the inclusion of additional hot stars. For this purpose, we have employed flux-calibrated spectra corresponding to representative spectral types and luminosity classes from the compilation of Pickles (1998). In particular, 43 spectra of O5–F0 stars with $6720 < T_{\text{eff}} < 39800$ K have been incorporated. It is worth noting that we have checked that no systematic offset is apparent between our $4000\,D$ measurements and those in Pickles' spectra. To display the range of stellar parameters covered by the resulting library, in Fig. 2 we present a $\log g - T_{\text{eff}}$ diagram of the calibrating stars.

4. Observations and data reduction

The stellar library was observed in a total of 13 observing runs from 1991 to 1996 using the JKT, INT and WHT at the Roque de los Muchachos Observatory (La Palma, Spain), the 3.5 m telescope at Calar Alto Observatory (Almería, Spain), and the 2.12 m telescope at San Pedro Mártir Observatory (Mexico). The bulk of the spectra (320 out of a total of 650 spectra) were taken in run 6, where the Richardson–Brealey Spectrograph was used to obtain 2.8 Å resolution spectra in the blue spectral range. A description of each observing run, including relevant observational configuration parameters, is given in Table 2. The number of stars observed in each run is quite variable since some of the runs were not devoted to the calibration of the break and, in these cases, only bright stars of the library were observed during twilight periods. The last column in Table 1 list the run numbers in which each star was observed.

The reduction of the data was performed with our own reduction package RED$_{\text{uc}}^{\text{uc}}$E[1] (Cardiel & Gorgas 1999), which allows a parallel treatment of data and error spectra (see below). We followed a standard reduction procedure for spectroscopic data: bias and dark subtraction, cosmic ray cleaning, flat-fielding, wavelength calibration, C-distortion correction, sky subtraction, atmospheric extinction correction and flux calibration (we did not attempt to obtain absolute fluxes since, as most line-strength indices, the break only requires relative fluxes). Cluster stars spectra were also corrected from interstellar reddening, using the color excesses quoted in Tables 4 and A3 from G93 and W94, respectively, and the averaged extinction curve of Savage & Mathis (1979).

In order to optimize the observing time during most of the runs, comparison arc frames were not taken next to each star observation. Instead of this, we only acquired arc exposures for a selected subsample of stars, which comprised objects with a complete coverage of all the spectral types and luminosity classes observed in each run. The wavelength calibration of the rest of the stars was performed by comparing them with the reference spectra. The repetition of this procedure with different reference spectra allow us to guarantee that wavelength calibration errors were always $\lesssim 0.2$ pixels.

5. Random errors and systematic effects

Since the aim of this paper is to derive an analytical representation of the behaviour of the D_{4000} as a function of effective temperature, metallicity and surface gravity, the sources of error are two-fold. In one hand, an important error source are the uncertainties in the adopted atmospheric stellar parameters. Detailed discussions of the

---

[1] See description of this package in:
http://www.ucm.es/info/Astrof/reduceme/reduceme.html

Table 2. Observational configurations

Run	Dates	Telescope[a]	Spectrograph	Detector	Disp.[b]	$\Delta\lambda$ [c]	FWHM[d]
1	1–3 Nov. 1991	WHT 4.2 m	ISIS blue arm	EEV#6	2.70	3500−6850	16.0
2	8–10 Jun. 1993	CAHA 3.5 m	CTS	TEK#12	3.46	3750−7350	7.2
3	2–6 Jul. 1994	INT 2.5 m	IDS 235 mm	TEK#3	3.30	3700−7100	5.2
4	9–10 Aug. 1994	CAHA 3.5 m	CTS	TEK#12	3.46	3700−7240	8.1
5	10–14 Sep. 1994	INT 2.5 m	IDS 235 mm	TEK#3	3.30	3700−7100	5.8
6	13–19 Feb. 1995	JKT 1.5 m	RBS	TEK#4	0.91	3600−4530	2.8
7	15 Feb. 1995	INT 2.5 m	IDS 235 mm	TEK#3	0.85	3634−4502	2.1
8	17–19 Dec. 1995	WHT 4.2 m	ISIS blue arm	TEK#1	2.90	3740−6700	12.3
9	15–16 Jan. 1996	CAHA 3.5 m	CTS	TEK#11	0.88	3654−4554	2.5
10	4 Aug. 1996	WHT 4.2 m	ISIS blue arm	TEK#2	1.53	3654−5219	4.9
11	28 Mar.–1 Apr. 1995	SPM 2.12 m	B&Ch	TEK	4.00	3500−7592	8.3
12	3 Mar. 1995	INT 2.5 m	IDS 500 mm	TEK#3	0.75	3670−4440	4.2
13	17–18 Nov. 1996	CAHA 3.5 m	CTS	SITe#6a	1.10	3569−5765	3.4

[a] JKT, INT and WHT (La Palma, Spain), CAHA (Calar Alto, Spain), SPM (San Pedro Mártir, Mexico),
[b] dispersion (Å/pixel),
[c] wavelength range (Å),
[d] measured spectral resolution (Å).

sources of the stellar parameters and their associated errors are given in the original papers G93 and W94. In this work we assume that these errors are random and, thus, their effect in the fitting procedure is minimized through the use of a library containing a large number of stars. The other type of errors are those associated to D_{4000} measurements, which are the subject of this section. Undoubtly, an accurate knowledge of the errors is essential to guarantee the validity of the final product of this work, i.e., the fitting functions of the break.

Since, apart from the cluster members, most of the stars of the Lick/IDS library are bright, and considering the low signal-to-noise ratio required to measure the D_{4000} with acceptable accuracy, systematic errors are the main source of uncertainty.

5.1. Random errors

(i) Photon statistics and read-out noise. With the aim of tracing the propagation of photon statistics and read-out noise, we followed a parallel reduction of data and error frames. For a detailed description on the estimation of random errors in the measurement of line-strength indices we refer the interested reader to Cardiel et al. (1998b). Starting with the analysis of the photon statistics and read-out noise, the reduction package RED$_{\mathrm{m}}^{\mathrm{uc}}$E is able to generate error frames from the beginning of the reduction procedure, and properly propagates the errors throughout the reduction process. In this way, important reduction steps such as flatfielding, geometrical distortion corrections, wavelength calibration and sky subtraction, are taken into account. At the end of the reduction process, each data spectrum $S(\lambda_i)$ has its associated error spectrum $\sigma(\lambda_i)$, which can be employed to derive accurate

index errors. The errors in the break are computed by (Cardiel et al. 1998b)

$$\Delta^2[D_{4000}]_{\mathrm{photon}} = \frac{\mathcal{F}_r \sigma^2_{\mathcal{F}_b} + \mathcal{F}_b \sigma^2_{\mathcal{F}_r}}{\mathcal{F}_b^4}, \tag{4}$$

with

$$\mathcal{F}_p \equiv \sum_{i=1}^{N_p} [\lambda_i^2 S(\lambda_i)], \tag{5}$$

and

$$\sigma^2_{\mathcal{F}_p} = \Theta^2 \sum_{i=1}^{N_p} [\lambda_i^4 \sigma^2(\lambda_i)], \tag{6}$$

where the subscripts b and r correspond, respectively, to the blue and red bandpasses of the break (p refers indistinctly to b or r), $S(\lambda_i)$ and $\sigma(\lambda_i)$ are the signal and the error in the pixel with central wavelength λ_i, Θ is the dispersion (in Å/pixel) assuming a linear wavelength scale, and N_p is the number of pixels covered by the p band (in general, fractions of pixels must be considered at the borders of the bandpasses). We have checked that the above analytical formulae exhibit an excellent agreement with numerical simulations. For the whole sample, the error of a typical observation introduced by these sources of noise is $\langle \Delta[D_{4000}]_{\mathrm{photon}} \rangle = 0.038$.

(ii) Flux calibration. During each run we observed a number (typically around 5) of different spectrophotometric standard stars (from Massey et al. 1988 and Oke 1990). The break was measured using the average flux calibration curve, and we estimated the random error in flux calibration as the rms scatter among the different D_{4000} values obtained with each standard. The typical error introduced by this uncertainty is $\langle \Delta[D_{4000}]_{\mathrm{flux}} \rangle = 0.034$.

(iii) Wavelength calibration and radial velocity correction. These two reduction steps are potential sources of

random errors in the wavelength scale of the reduced spectra. Radial velocities for field stars were obtained from the Hipparcos Input Catalogue (Turon et al. 1992), which in the worst cases are given with mean probable errors of ~ 5 km s^{-1} (~ 0.07 Å at $\lambda 4000$ Å). For the cluster stars, we used either published radial velocities for individual stars, if available, or averaged cluster radial velocities (Hesser et al. 1986: M 3, M 5, M 10, M 13, M 71, M 92, NGC 6171; Friel 1989: NGC 188; Friel & Janes 1993: M 67, NGC 7789; Turon et al. 1992: Coma, Hyades). Typical radial velocity errors for the cluster stars are $\lesssim 15$ km s^{-1} (~ 0.2 Å at $\lambda 4000$ Å). To have an estimate of the random error introduced by the combined effect of wavelength calibration and radial velocity, we cross-correlated fully calibrated spectra corresponding to stars of similar spectral types. The resulting typical error is 20 km s^{-1}, being always below 75 km s^{-1}. This translates into a negligible error of $\langle \Delta [D_{4000}]_{\mathrm{wavelength}} \rangle = 0.003$. However, it may be useful to estimate the importance of this effect when measuring the break in galaxies with large radial velocity uncertainties. As a reference, using the 18 spectra displayed in Fig. 3, a velocity shift of ~ 100 km s^{-1} translates into relative D_{4000} errors always below 1%. Furthermore, for K0 III stars we obtain $\Delta [D_{4000}]_{\mathrm{wavelength}} \simeq 1.56\ 10^{-4} \Delta v$, where Δv is the velocity error in km s^{-1} (this relation only holds for $\Delta v \leq 150$ km s^{-1}; for Δv in the range from $150 - 1000$ km s^{-1} the error increases slower, and remains below 0.1).

(iv) Additional sources of random errors. Expected random errors for each star can be computed by adding quadratically the random errors derived from the three sources previously discussed, i.e.,

$$\Delta^2[D_{4000}]_{\mathrm{expected}} =$$

$$\Delta^2[D_{4000}]_{\mathrm{photon}} + \Delta^2[D_{4000}]_{\mathrm{flux}} + \Delta^2[D_{4000}]_{\mathrm{wavelength}}. \quad (7)$$

However, additional (and unknown) sources of random error may still be present in the data. Following the method described in González (1993), we compared, within each run, the standard deviation of the D_{4000} measurements of stars with multiple observations with the expected error $\Delta[D_{4000}]_{\mathrm{expected}}$. For those runs in which the standard deviation was significantly larger than the expected error (using the F-test of variances with a significance level $\alpha = 0.3$), a residual random error $\Delta_{\mathrm{residual}}$ was derived and added to all the individual stellar random errors:

$$\Delta^2[D_{4000}]_{\mathrm{random}} =$$

$$\Delta^2[D_{4000}]_{\mathrm{expected}} + \Delta^2[D_{4000}]_{\mathrm{residual}}. \quad (8)$$

It is worth noting that this additional error was only needed for some runs. In the particular case of run 6, with a large number (54) of stars with multiple observations, the agreement between expected and measured error was perfect.

5.2. Systematic effects

The main sources of systematic effects in the measurement of spectral indices in stars are spectral resolution, sky subtraction and flux calibration.

(i) Spectral resolution. We have examined the effect of instrumental broadening in the break by convolving the 18 spectra of Fig. 3 with a broadening function of variable width. The result of this study indicates that, as expected, the break is quite insensitive to spectral resolution. As a reference, for a spectral resolution of 30 Å (FWHM) the effect in the break is below 1%. Therefore, given the resolutions used in this work (last column in Table 2) no corrections are needed in any case.

(ii) Sky subtraction. Since the field giant and dwarf stars of the library are bright, the exposure times were short enough to neglect the effect of an anomalous subtraction of the sky level. However, most of the cluster stars are not bright, being necessary exposures times of up to 1800 seconds for the faintest objects. In addition, the observation of these stars, specially those in globular clusters, were performed with the unavoidable presence of several stars inside the spectrograph slit, which complicated the determination of the sky regions. In Cardiel et al. (1995) we already studied the systematic variations on the D_{4000} measured in the outer parts of a galaxy (where light levels are only a few per cent of the sky signal) due to the over– or under–estimation of the sky level. We refer the interested reader to that paper for details. Although there is not a simple recipe to detect this type of systematic effect, unexpectedly high D_{4000} values in faint cluster stars can arise from an anomalous sky subtraction.

(iii) Flux calibration. Due to the large number of runs needed to complete the whole library, important systematic errors can arise due to possible differences among the spectrophotometric system of each run. In order to guarantee that the whole dataset is in the same system, we compared the measurements of the stars in common among different runs. Since run 6 was the observing run with the largest number of stars (including numerous multiple observations) and with reliable random errors (see above), we selected it as our spectrophotometric reference system. Therefore, for each run we computed a mean offset with run 6, which was introduced when it was significantly different from 0 (using a t test). It is important to highlight that differences between a *true* spectrophotometric system and that adopted in this work may still be present. Therefore, we encourage the readers interested in the predictions of the present fitting functions, to include in their observations a number of template stars from the library to ensure a proper correction of the data.

5.3. Final errors

The comparison of measurements of the same stars in different runs also provides a powerful method to refine the
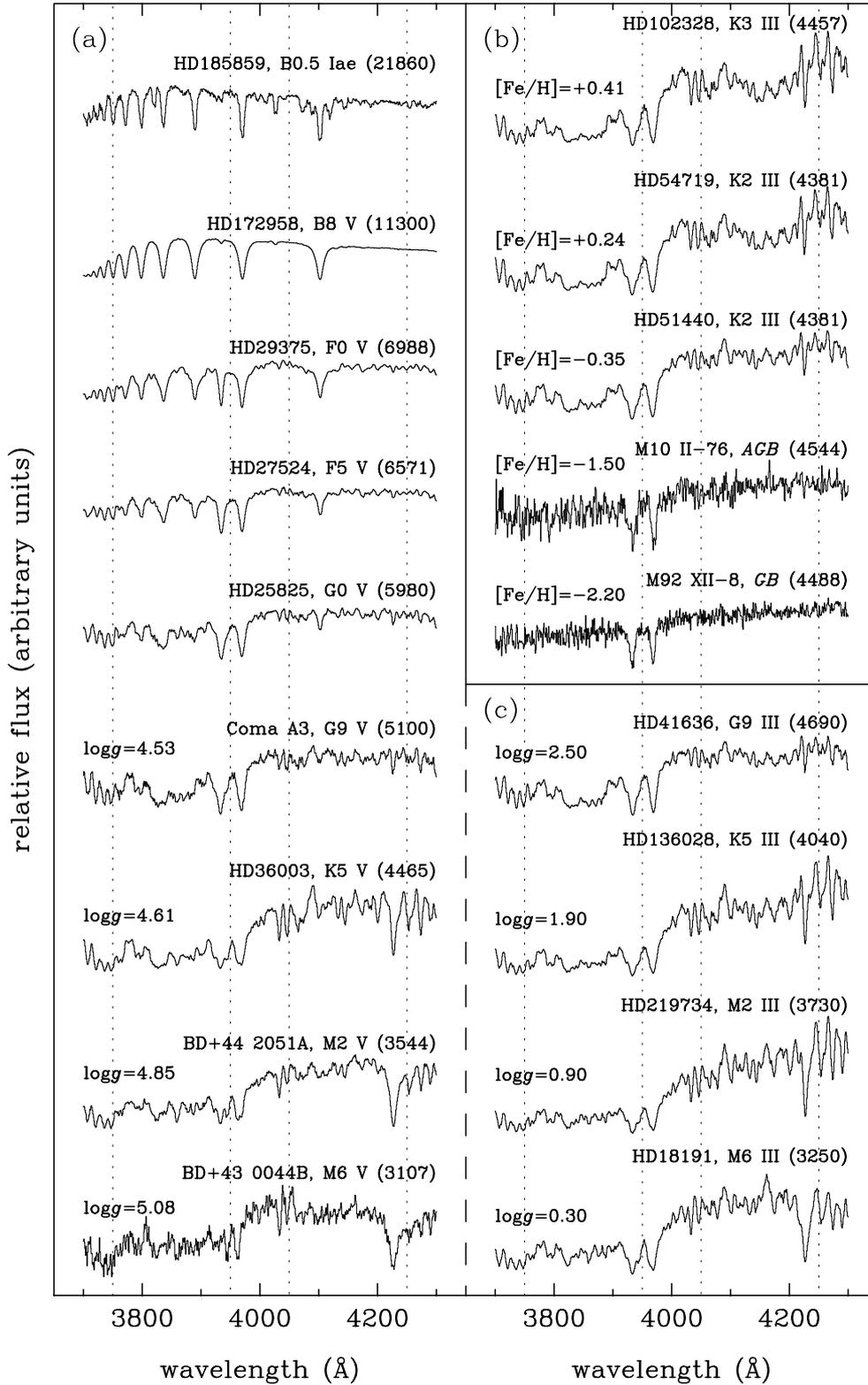
Fig. 3. Sample spectra of stars observed in run 6. Effective temperatures are given in parenthesis. Panel **a)** is a sequence in spectral types for main sequence stars. Panel **b)** shows stars with similar temperature but with a wide range in metallicity. Panel **c)** displays a sequence in spectral types for giant stars, which can be compared with the lower part of the dwarf sequence in panel **a)**
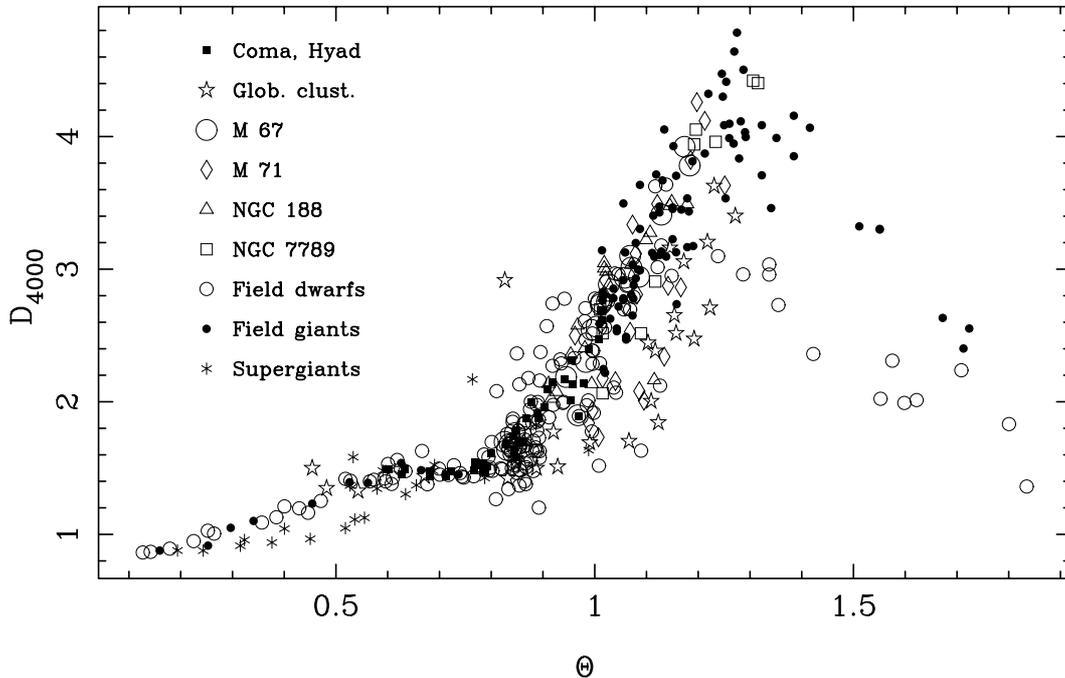
Fig. 5. D_{4000} as a function of $\theta \equiv 5040/T_{\mathrm{eff}}$ for the sample, together with the derived fitting functions. Stars of different metallicities are shown with different symbol types, with sizes giving an indication of the surface gravity (in the sense that low-gravity stars, i.e. giants, are plotted with larger symbols). Concerning the fitting functions, in the low θ range, the solid line corresponds to dwarf and giant stars, whereas the dashed line is used for supergiants. For lower temperatures, thick and thin lines refer to giant and dwarf stars respectively. For each of these groups in the mid-temperature range, the different lines represent the metallicities [Fe/H] $= +0.5, 0, -0.5, -1, -1.5, -2$, from top to bottom

and

$$D_{4000}(\theta, [\mathrm{Fe/H}], \log g) = \mathrm{const.} + e^{p(\theta, [\mathrm{Fe/H}], \log g)}, \quad (12)$$

where p is a polynomial with terms up to the third order, including all possible cross-terms among the parameters:

$$p(\theta, [\mathrm{Fe/H}], \log g) = \sum_{k=0}^{19} c_k \, \theta^i \, [\mathrm{Fe/H}]^j \, (\log g)^l, \quad (13)$$

with $0 \leq i + j + l \leq 3$.

The polynomial coefficients were determined from a least squares fit where all the stars were weighted according to the D_{4000} observational errors listed in Table 1. Note that this is an improvement over the procedure employed by G93 and W94 for the Lick indices.

Obviously, not all possible terms are necessary. The strategy followed to determine the final fitting function is the successive inclusion of terms, starting with the lower powers. At each step, the term which yielded a lower new residual variance was tested. The significance of this new term, as well as those of all the previously included coefficients, was computed using a t-test (i.e. from the error in the coefficient, we tested whether it was significantly different from zero). Note that this is equivalent to performing a F-test to check whether the unbiased residual variance is significantly reduced with the inclusion of the additional term. Following this procedure, and using typically a significant level of $\alpha = 0.10$, only statistically

significant terms were retained. The problem is well constrained and, usually, after the inclusion of a few terms, a final residual variance is asymptotically reached and the higher order terms are not statistically significant. Throughout this fitting procedure we also kept an eye on the residuals to assure that no systematic behaviour for any group of stars (specially stars from any given cluster or metallicity range) was apparent.

After a set of trial fits, it was clear that temperature is the main parameter governing the break. Unfortunately, the behaviour of the D_{4000} could not be reproduced by a unique polynomial function in the whole temperature range spanned by the library, forcing us to divide the temperature interval into several regimes. The derived composite fitting function is shown in Fig. 5. In Table 3 we list the corresponding coefficients and errors, together with the typical error of the N stars used in each interval ($\sigma_{\mathrm{typ}}^2 = N/\sum_{i=1}^n \sigma_i^{-2}$), the unbiased residual variance around the fit (σ_{std}^2) and the determination coefficient (r^2).

In the high temperature regime ($\theta \leq 0.75$, $T_{\mathrm{eff}} \geq 6700$ K) a dichotomic behaviour for dwarfs and giants on one side, and supergiants on the other, is clearly apparent. Therefore we derived different fitting functions for each gravity range. For the first group the amplitude of the break is quite constant and only the linear term in θ is
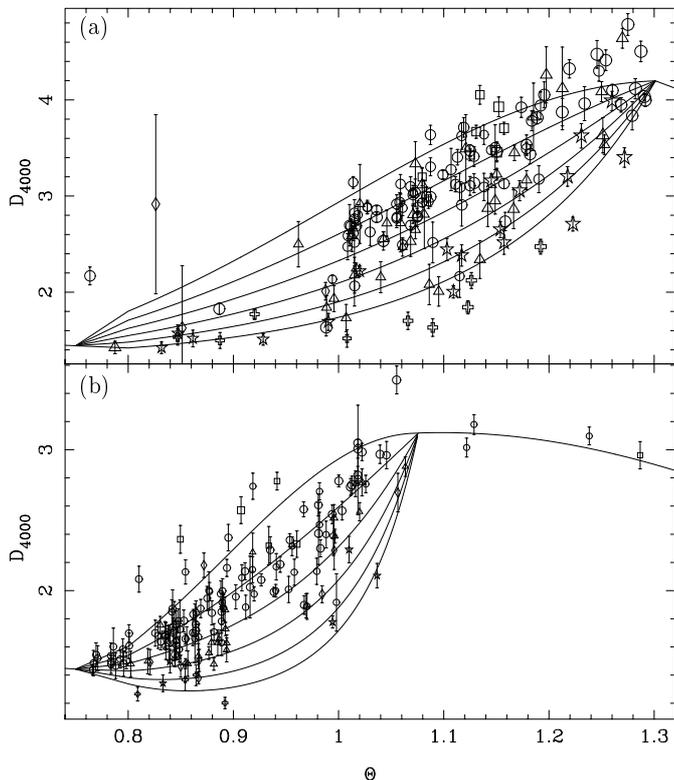
Fig. 6. Details of the fitting functions in the mid-temperature range for **a)** giant ($\log g < 3.5$) and **b)** dwarf ($\log g > 3$) stars. See caption to Fig 5. Error bars for the D_{4000} measurements are also shown

statistically significant (note that we subdivide this range in two intervals to achieve a better fit). The independence on metallicity is naturally expected (see Sect. 2) but note that an important fraction of the stars in this range either lack of a [Fe/H] estimation or are restricted to the solar value.

The behaviour of the cool stars ($0.75 \leq \theta \leq 1.3$, 3900 K $\leq T_{\rm eff} \leq 6700$ K) is more complex and [Fe/H] terms are clearly needed. On the other hand, no gravity term is significant. However, whilst for the giant stars D_{4000} increases with θ all the way up to $\theta \approx 1.3$, for higher gravities it reaches a maximum at $\theta \approx 1.1$ and then levels off. Furthermore, separate fits for dwarfs and giants in this $T_{\rm eff}$ range (with a gravity cutoff around $3 - 3.5$) yield residual variances that are significantly smaller than the variance from a single fit. Hence, we have derived different fitting functions for dwarfs and giants. This dichotomic behaviour of the break is not surprising since its strength is quite dependent on the depth of the CN bands (Fig. 1) which also shows a similar behaviour (G93) due to the onset of the dredge-up processes at the bottom of the giant branch. In Fig. 6 we show in detail the fitting functions derived for each gravity group in this temperature range.

Concerning the cold stars ($\theta \geq 1.3$, $T_{\rm eff} \leq 3900$ K), the difference between giants and dwarfs is quite evident and
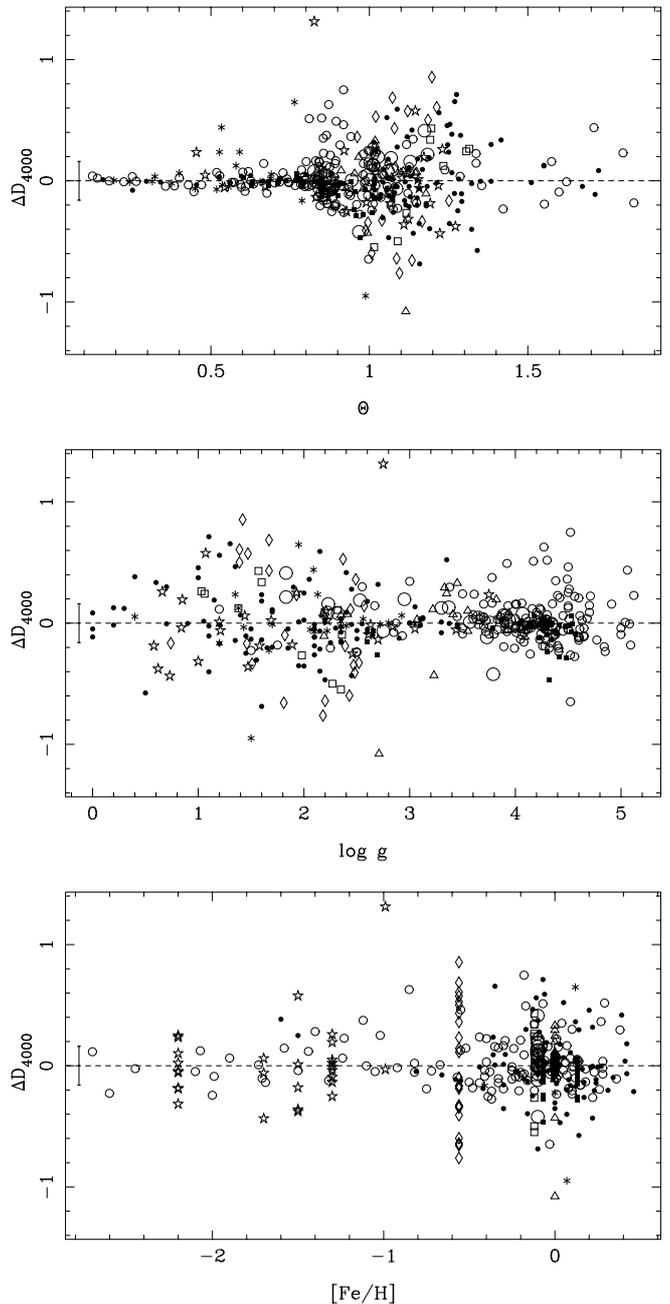
Fig. 7. Residuals of the derived fitting functions (observed minus predicted) against the three input stellar parameters. Symbol types are the same as in Fig. 3. The length of the error bar is twice the unbiased residual standard deviation

two fitting functions have been derived (see also Sect. 2). Again, the metallicity terms are not significant, although this may be, at least in part, due to the paucity of input metallicities in this range. It must be noted that the different fitting functions have been constructed with the constrain of allowing for a smooth transition in the predicted D_{4000} indices among the different $T_{\rm eff}$ and gravity ranges.

Table 3. Parameters of the empirical fitting functions in each temperature and gravity range

Hot stars		$0.12 < \theta < 0.63$			$3 < \log g < 4.5$
polynomial fit					$N = 39$
c_0	:	0.6548	$\pm$	0.0222	$\sigma_{\mathrm{typ}} = 0.041$
θ	:	1.340	$\pm$	0.049	$\sigma_{\mathrm{std}} = 0.046$
					$r^2 = 0.96$
Warm stars		$0.63 < \theta < 0.75$			$3 < \log g < 4.5$
polynomial fit					$N = 23$
c_0	:	1.823	$\pm$	0.140	$\sigma_{\mathrm{typ}} = 0.051$
θ	:	-0.5068	$\pm$	0.2030	$\sigma_{\mathrm{std}} = 0.034$
					$r^2 = 0.35$
Hot supergiants		$0.19 < \theta < 0.69$			$0 < \log g < 3$
polynomial fit					$N = 18$
c_0	:	0.8613	$\pm$	0.0328	$\sigma_{\mathrm{typ}} = 0.041$
θ^3	:	1.849	$\pm$	0.211	$\sigma_{\mathrm{std}} = 0.079$
					$r^2 = 0.87$
Cool dwarfs		$0.75 < \theta < 1.08$			$3 < \log g < 5.1$
exponential fit (const. $= 0.9$)					$N = 161$
c_0	:	-8.154	$\pm$	2.007	$\sigma_{\mathrm{typ}} = 0.068$
θ	:	13.45	$\pm$	4.28	$\sigma_{\mathrm{std}} = 0.178$
[Fe/H]	:	-17.06	$\pm$	7.28	$r^2 = 0.88$
θ [Fe/H]	:	38.12	$\pm$	15.80	
θ^2	:	-4.769	$\pm$	2.269	
θ^2 [Fe/H]	:	-20.69	$\pm$	8.52	
Cool giants		$0.75 < \theta < 1.30$			$0 < \log g < 3.5$
exponential fit (const. $= 0.9$)					$N = 176$
c_0	:	-5.665	$\pm$	1.563	$\sigma_{\mathrm{typ}} = 0.081$
θ	:	9.279	$\pm$	2.766	$\sigma_{\mathrm{std}} = 0.261$
[Fe/H]	:	-3.273	$\pm$	2.274	$r^2 = 0.85$
θ [Fe/H]	:	7.322	$\pm$	4.266	
θ^2	:	-3.080	$\pm$	1.218	
θ^2 [Fe/H]	:	-3.694	$\pm$	1.986	
Cold dwarfs		$1.08 < \theta < 1.83$			$4.5 < \log g < 5.2$
exponential fit (const. $= 1.15$)					$N = 15$
c_0	:	-2.908	$\pm$	2.949	$\sigma_{\mathrm{typ}} = 0.078$
θ	:	6.535	$\pm$	4.243	$\sigma_{\mathrm{std}} = 0.194$
θ^2	:	-2.976	$\pm$	1.506	$r^2 = 0.83$
Cold giants		$1.30 < \theta < 1.72$			$0 < \log g < 1.2$
polynomial fit					$N = 15$
c_0	:	9.525	$\pm$	0.742	$\sigma_{\mathrm{typ}} = 0.083$
θ	:	-4.094	$\pm$	0.486	$\sigma_{\mathrm{std}} = 0.211$
					$r^2 = 0.92$

Table 4. Uncertainties in the predicted D_{4000} values for some indicative sets of stellar parameters. For the cool stars ($T_{\mathrm{eff}} \leq 6000$ K) the term *giants* refers also to supergiant stars

T_{eff}	[Fe/H]	dwarfs–giants	supergiants
30000		0.015	0.032
12000		0.008	0.023
7500		0.010	0.044
		dwarfs	giants
6000	0.5	0.045	0.156
6000	0.0	0.024	0.099
6000	-1.0	0.031	0.075
6000	-2.0	0.043	0.105
5000	0.5	0.103	0.079
5000	0.0	0.044	0.043
5000	-1.0	0.082	0.053
5000	-2.0	0.119	0.073
4000	0.5		0.167
4000	0.0	0.125	0.088
4000	-1.0		0.173
4000	-2.0		0.322
3200		0.094	0.082

a 2.5 factor larger than what should be expected solely from measurement errors. Since we are quite confident that these latter errors are realistic (see Sect. 5), and although some scatter may arise from the fact than the fitting functions are not able to reproduce completely the complex behaviour of the D_{4000}, most of the extra scatter must arise form uncertainties in the input atmospheric parameters. For example, the residual D_{4000} scatter of 0.248 for the cool giants (at $\theta = 1.0$ and [Fe/H] $= 0.0$) can be fully explained by the combined effect of a 166 K uncertainty in T_{eff} and a 0.29 dex error in [Fe/H], both consistent with the typical errors found by Soubiran et al. (1998) when comparing atmospheric parameters from the literature. Another quantitative measurement of the quality of the present fitting functions is the determination coefficient for the whole sample $r^2 = 0.96$. This indicates that a 96% of the original variation of the break in the sample is explained by the derived fitting functions.

Since the goal of this work is to predict reliable D_{4000} indices for any given combination of input atmospheric parameters, we have investigated, using the covariance matrices of the fits, the random errors in such predictions. These errors are given in Table 4 for some representative sets of input parameters. Note that, as it should be expected, the uncertainties are smaller for near-solar metallicities. Interestingly, although the library does not include a high number of 0–B stars, the predicted indices at the hot end of the star sample are rather reliable.

In Fig. 7 we plot the residuals from the fits as a function of effective temperature, metallicity and gravity. Note that no trends are apparent with any of these parameters. We have also checked for systematic residuals within any of the star clusters. Except for an unexplained negative offset for the Coma stars ($\Delta D_{4000} = 0.09$, not due to an error in the adopted metallicity), no systematic offsets have been found. For the 420 stars used in the fit, we derive an unbiased residual standard deviation $\sigma_{\mathrm{std}} = 0.160$. This must be compared with the typical error in the D_{4000}, $\sigma_{\mathrm{typ}} = 0.064$. Therefore, the residuals are, in the mean,

8. Summary

We have derived a set of empirical fitting functions describing the behaviour of the break at $\lambda 4000$ Å in terms of the atmospheric stellar parameters: effective temperature, metallicity and surface gravity. This calibration can be easily incorporated into stellar population models to provide accurate predictions of the D_{4000} for composite systems. In a forthcoming paper we will analyze the measurements of the break in old stellar populations at the light of the predictions of such models. Considering the volume covered by the employed stellar library (Lick/IDS + Pickles' hot subsample) in the stellar parameter space, the derived fitting functions suit the requirements to provide accurate D_{4000} predictions for populations with ages larger than about 0.1 Gyr, and $-1 \leq [\text{Fe/H}] \leq +0.5$ dex (see also W94). Note however that, since the break could be contaminated by nebular emission in galaxies with ongoing star formation, it is necessary to include this effect in the population modelling in order to predict reliable D_{4000} indices for such stellar populations. It should also be noted that the applicability of the derived fitting functions is safe as far as the abundance ratios of the library stars reflect those in the modeled stellar populations.

In order to facilitate the usage of the present D_{4000} fitting functions we have written a FORTRAN subroutine, available from:

http://www.ucm.es/info/Astrof/D4000/D4000.html

This routine computes the value of the D_{4000} as a function of the input stellar parameters T_{eff}, [Fe/H] and $\log g$. The code performs smooth interpolations among temperature and gravity ranges, providing also an estimate of the error in the predicted index,

References

Abraham R.G., Smecker–Hane T.A., Hutchings J.B., et al., 1996, ApJ 471, 694

Barbaro G., Poggianti B.M., 1997, A&A 324, 490

Belloni P., Bruzual A.G., Thimm G.J., Roser H.-J., 1995, A&A 297, 61

Bressan A., Chiosi C., Tantalo R., 1996, A&A 311, 425

Bruzual A.G., 1983, ApJ 273, 105

Bruzual A.G., Charlot S., 1996 (in preparation)

Burstein D., Faber S.M., Gaskell C.M., Krumm N., 1984, ApJ 287, 586

Burstein D., Faber S.M., González J.J., 1986, AJ 91, 1130

Carbon D.F., Langer G.E., Butler D., et al., 1982, ApJS 49, 207

Cardiel N., 1999, Ph.D. thesis, Universidad Complutense de Madrid, Spain

Cardiel N., Gorgas J., 1999 (in preparation)

Cardiel N., Gorgas J., Aragón-Salamanca A., 1995, MNRAS 277, 502

Cardiel N., Gorgas J., Aragón-Salamanca A., 1998a, MNRAS 298, 977

Cardiel N., Gorgas J., Cenarro J., González J.J., 1998b, A&AS 127, 597

Charlot S., Silk J., 1994, ApJ 432, 453

Charlot S., Ferrari F., Mathews G.J., Silk J., 1993, ApJ 419, L57

Davidge T.J., Clark, C.C., 1994, AJ 107, 946

Davidge T.J., Grinder M., 1995, AJ 109, 1433

Dressler A., 1987, in Nearly Normal Galaxies: From the Planck Time to the Present, Faber S.M. (ed.). New York: Springer-Verlag, p. 276

Dressler A., Gunn J.E., 1990, in Evolution of the Universe of Galaxies, Kron R.G. (ed.) ASP Conf. Ser. 10, 200

Dressler A., Shectman S.A., 1987, AJ 94, 899

Faber S.M., 1973, ApJ 179, 731

Faber S.M., Friel E.D., Burstein D., Gaskell C.M., 1985, ApJS 57, 711

Friel E.D., 1989, PASP 101, 244

Friel E.D., Janes K.A., 1993, A&A 267, 75

González J.J., 1993, Ph.D. thesis, University of California, Santa Cruz

Gorgas J., Faber S.M., Burstein D., et al., 1993, ApJS 86, 153 (G93)

Hamilton D., 1985, ApJ 297, 371

Hammer F., Flores H., Lilly S.J., et al., 1997, ApJ 481, 49

Hesser J.E., 1986, PASP 98, 403

Johnstone R.M., Fabian A.C., Nulsen P.E.J., 1987, MNRAS 224, 75

Jones L.A., Worthey G., 1995, ApJ 446, L31

Kimble R.A., Davidsen A.F., Sandage A.R., 1989, Ap&SS 157, 237

Lang K.R., 1974, Astrophysical Formulae. Springer-Verlag, New York, p. 175

Laurikainen E., Jaakkola T., 1985, Ap&SS 109, 111

Longhetti M., Rampazzo R., Bressan A., Chiosi C., 1998, A&AS 130, 251

Massey P., Strobel K., Barnes J.V., Anderson E., 1988, ApJ 328, 315

McClure R.D., van den Bergh S., 1968, AJ 73, 313

Moore C.E., Minnaert M.G., Houtgast J., 1966, The solar spectrum 2935 Å to 8770 Å, National Bureau of Standards Monograph, Washington

Morgan W.W., 1959, AJ 64, 432

Munn J.A., 1992, ApJ 399, 444

Oke J.B., 1990, AJ 99, 1621

Pickles A.J., 1985, ApJS 59, 33

Pickles A.J., 1998, PASP 110, 863

Poggianti B.M., Barbaro G., 1997, A&A 325, 1025

Ponder J.M., Burstein D., O'Connell R.W., et al., AJ 116, 2297

Rakos K.D., Schombert J.M., Kreidl T.J., 1991, ApJ 377, 382

Rose J.A., 1984, AJ 89, 1238

Rose J.A., 1994, AJ 107, 206

Savage B.D., Mathis J.S., 1979, ARA&A 17, 73

Smith G.H., Shetrone D., Briley M.M., Churchill C.W., Bell R.A., 1997, PASP 109, 236

Songaila A., Cowie L.L., Hu E.M., Gardner J.P., 1994, ApJS 94, 461

Soubiran C., Katz D., Cayrel R., 1998, A&AS 133, 221

Spinrad H., 1980, in IAU Symp. 92, Objects at High Redshift, Abell G.O. & Peebles P.J.E. (eds.). Dordrecht: Reidel, p. 39

Spinrad H., 1986, PASP 98, 269

Straizys V., Sviderskiene Z., 1972, Bull. Vilnius An. Obs. 35, 1

Trager S.C., Worthey G., Faber S.M., Burstein D., González J.J., 1998, ApJS 116, 1

Tripicco M.J., 1989, AJ 97, 735

Turon C., et al., 1992, The Hipparcos Input Catalogue, ESA SP-1136

van den Bergh S., 1963, AJ 68, 413

van den Bergh S., Sackmann I.J., 1965, AJ 70, 353

Vazdekis A., Arimoto N., 1999, ApJ (submitted)

Vazdekis A., Casuso E., Peletier R.F., Beckman J.E., 1996, ApJS 106, 307

Wildey R.L., Burbidge E.M., Sandage A.R., Burbidge G.R., 1962, ApJ 135, 94

Worthey G., 1994, ApJS 95, 107

Worthey G., Ottaviani D.L., 1997, ApJS 111, 377

Worthey G., Faber S.M., González J.J., Burstein D., 1994, ApJS 94, 687 (W94)